SAR and Optical Data Fusion for Change Detection

Conference Paper · May 2007

DOI: 10.1109/URS.2007.371770 · Source: IEEE Xplore

CITATIONS
8

READS
250

4 authors, including:

Pierfrancesco Lombardo
Sapienza University of Rome
276 PUBLICATIONS **3,364** CITATIONS
SEE PROFILE

Marine Costantini
School of Social Work and Health
53 PUBLICATIONS **1,499** CITATIONS
SEE PROFILE

2007 Urban Remote Sensing Joint Event

SAR and Optical Data Fusion for Change Detection

F. Orsomando, P. Lombardo
Dept. INFOCOM
University of Rome"La Sapienza"
Rome, Italy
fede.79@fastwebnet.it; lombardo@infocom.uniroma1.it

M. Zavagli, M. Costantini
Earth Observation Department
Telespazio S.p.A
Rome, Italy
mario.costantini@telespazio.com

***Abstract*— In this work, we devise a change detection technique for urban areas based on the fusion of temporal series of SAR images with a single multi-band optical image. The proposed technique aims at exploiting both the high repetition observation rate available with the new generation of SAR systems and the high level of details available even in a single multiband optical image. The approach has been validated by using a multitemporal set of ENVISAT SAR images and a couple of QuickBird optical images, that are also used to provide evidence on the changes by visual inspection at high resolution. The preliminary results shown in the paper show the potentiality of the joint processing of SAR and optical images.**

I. INTRODUCTION

Remote sensing images required to detect changes, especially in urban areas, must be both temporally close one to another and rich in details. These two conditions are rarely satisfied when only SAR or only optical data are used. Although available with high temporal frequency - since not affected by illumination and atmospheric conditions -, SAR images do not allow a sharp definition of shapes and edges of the changed areas because of the presence of speckle. In contrast, optical images that are rich of details and allow the detection of sharp edges, are usually not frequently available. Therefore, appropriate techniques able to obtain the fusion between the data of the two sensors are of major interest to exploit at the same time both the SAR and the multi-spectral optical images, thus combining their respective strengths [1].

The combined exploitation of the information available in optical and SAR images is very difficult when dealing directly with change detection, due to the two different physical imaging mechanisms. In contrast, the change detection is naturally conceived on a multitemporal sequence of SAR images. Therefore, we do not attempt to use the optical images inside the change detection test, but we use them to achieve a high quality segmentation of the set of images before applying change detection. The optical images are especially suitable to provide reliable segmentations with a high level of details, and as such can contribute, together with the SAR images, to a final high quality result. If the presence of optical images is successful in providing a segmentation closer to the truth, an improved change detection can be achieved. In fact, based on the jointly defined mask of segments, the change detection can exploit all the SAR image pixels in each true homogeneous segment, thus removing the effect of speckle and intrinsic fluctuations inside the SAR reflectivity maps. In this preliminary work, only a step pattern is supposed for the change and no further "a priori" knowledge about the change times and RCS levels of the change are exploited.

The proposed change detection technique is especially suitable for urban areas, where the aim is to detect buildings under construction, or both natural and human destructions of buildings and infrastructures, which are characterized by small size and potentially a fast change rate. In particular, the identification of the shape of the changed areas is of primary interest, since it is the first step for the identification and recognition of portions of buildings or infrastructures that have been modified. To this purpose, the high accuracy in the determination of edges is also extremely important, because it allows to identify also changes of limited size.

The presented change detection technique is analyzed and validated by application to a set of real data of the urban environment (ENVISAT SAR and Quick Bird optical images). A map of the ground-truths is obtained through visual comparison of two high-resolution optical images acquired at two different times, respectively close to the start and the end of the sequence of SAR images. Moreover, to assess the performance improvement achievable by using a single multi-band optical image together with a sequence of SAR images, two different data sets have been considered as input to the change detection algorithm:

- a temporal series of only SAR images;
- a temporal series of SAR images, plus a single multi-band optical image.

The comparison of the results obtained by processing the two datasets allows us to assess the improvement made available by the addition of the optical image, and thus making conclusions on the potential impact of data fusion for the change detection in the urban environment.

The paper is organized as follows. Section II, describes the proposed technique to detect the temporal changes on a segment-to segment basis. In section III, two multi-temporal segmentation techniques are described, which are used as the preliminary basic step required before the application of the change detection algorithm. The application to the real data sets and the validation results are reported in section IV. Finally, in section V we draw some conclusions.

1-4244-0712-5/07/$20.00 ©2007 IEEE.

II. CHANGE DETECTION TECHNIQUE

To detect changes in the monitored area, we operate on the multitemporal sequence of SAR images, with the aim to compare the intensity values at different times to identify positions where permanent changes have been introduced. Since the SAR images are largely affected by multiplicative speckle noise, also the change detection results are very likely to be dependent on speckle. To reduce its effect on the overall performance, the analysis of the temporal evolution of the statistical parameters of the backscattering coefficients is not carried out on a pixel-by-pixel basis, but on homogeneous regions. Therefore, following the techniques developed in references [2], [3], the applied change detection technique is applied after a SAR segmentation stage, which must be rich in details and must derive its segments from all involved SAR data. This segmentation can highly benefit from the presence of at least a multi-band optical image, to increase the level of details and to find the correct edges (Figure 1). Before describing the segmentation stage, we recall the used change detection approach and its derivation.

To derive the change detection technique, we start from the following statistical model for the temporal series of M SAR images. Let the generic image be described by a disjoint set of P non-overlapping segments S_j, $j=1,...,P$. Each segment S_j, of N_j pixels is characterized by the vector $(\sigma_{j,1}, \sigma_{j,2},..., \sigma_{j,M})$, where $\sigma_{j,i}$ is the expected value of the pixel intensity for the segment S_j in the i^{th} SAR image.

A simple statistical model for the probability density function (pdf) of the intensities $x_{n,i}$ $n=1, ...,N_j, i=1, ..., M$ in the *j-th* homogeneous regions of SAR images, which also yields a straightforward way to derive the desired change detection technique, is to characterize them with the Gamma pdf. In particular, the Gamma variables have average values $(\sigma_{j,1}, \sigma_{j,2},..., \sigma_{j,M})$, and order parameter ν equal to the number of looks L, [4]:

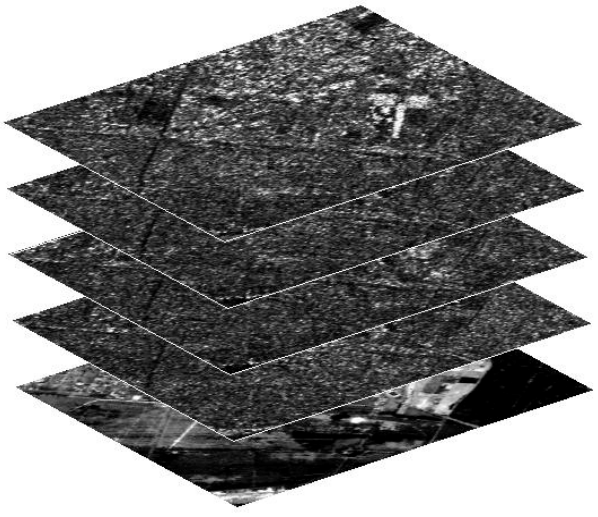

Figure 1: Stack of some SAR images and one optical image temporally sorted

$$p_{x^{(j)}}\left(\{x_{n,i}\}\right)=\prod_{n=1}^{N_j}\prod_{i=1}^{M}\frac{1}{\Gamma(\nu)}\left(\frac{\nu}{\sigma_{j,i}}\right)^{\nu} x_{n,i}^{\nu-1}\ \exp\left(-\frac{\nu}{\sigma_{j,i}}x_{n,i}\right) \qquad (1)$$

Both spatial and temporal statistical independence is supposed for pixels within the same homogeneous region (though showing the same properties of the distribution). Therefore, the sample mean values $\eta_{j,i}, j=1,...,P;\ i=1, ...M,$ estimated over the N_j pixels of the *j-th* segment follow themselves the Gamma pdf with the same average value and order parameter equal to νN_j.

In order to achieve a simplified definition of an abrupt change, we assume a step pattern of reflectivities without any "a priori" knowledge about the change time. We also assume no knowledge about the RCS levels before and after the change. Based on this simple model, two hypotheses can be formulated for the generic segment S_j with N_j pixels, (as shown in the Figure 2:

α) Step pattern: $\sigma_{j,i}=\sigma_{jA}$ for $i=1,...,m$, $\sigma_{j,i}=\sigma_B$ for $i=m+1,...,M$,

β) Constant pattern: $\sigma_{j,i}=\sigma_0$ for $i=1,...,M$.

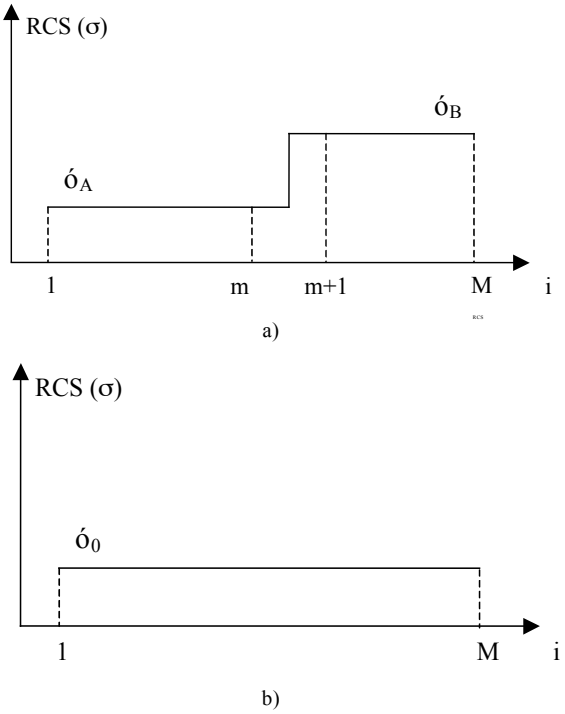

Figure 2: Possible patterns of the RCS temporal series: a) step pattern and b) constant pattern.

Following the assumptions above, the RCS values σ_A, σ_B, σ_0 and the change time m are unknown. Based on the model in eq. (1), the following generalized likelihood functions are obtained for the j-th segment, respectively under hypothesis α and β:

$$\lambda_{\alpha}^{(j)}=\prod_{i=1}^{m}\hat{\sigma}_a^{-\nu N_j}\exp\left(-\frac{\nu N_j}{\hat{\sigma}_a}\eta_{j,i}\right)\prod_{i=m+1}^{M}\hat{\sigma}_b^{-\nu N_j}\exp\left(-\frac{\nu N_j}{\hat{\sigma}_b}\eta_{j,i}\right) \qquad (2)$$

$$\lambda_{\beta}^{(j)} = \prod_{i=1}^{M} \hat{\sigma}_0^{-\nu N_j} \exp\left(-\frac{\nu N_j}{\hat{\sigma}_0} \eta_{j,i} \right) \tag{3}$$

where $\hat{\sigma}_A$, $\hat{\sigma}_B$ and $\hat{\sigma}_0$ are respectively the maximum likelihood (ML) estimates of the three parameters σ_A, σ_B and σ_0. The maximization of the likelihood ratio $\lambda_{ab} = \lambda_a/\lambda_b$ with respect to m (it is worth noting that $\hat{\sigma}_A$ and $\hat{\sigma}_B$ depend on m) allows to decide, for each segment, between hypothesis α and hypothesis β. In particular, by selecting an appropriate detection threshold λ, if $\lambda_{ab} > \lambda$, the hypothesis α is accepted and therefore a change is recognized in the segment under analysis, otherwise ($\lambda_{ab} < \lambda$), the hypothesis β is selected and no changes are detected. The threshold λ is determined as function of the change time m and of the segment size N_i by imposing a given probability of false alarm evaluated by using the pdf in eq. (3), [2][3].

The test above allows to decide, whether or not a change has taken place in each segment. This is clearly obtained only using the sequence of SAR images. However, SAR images and optical images can be jointly used to identify the shape and size of the homogeneous segments, which allows the full exploitation of their information content

III. Joint Segmentation Technique for Multitemporal SAR and Optical Images

As introduced above, the proposed approach decides for a change by exploiting the temporal series of SAR images. To reduce the effect of speckle noise on the detection of changes, the analysis of the temporal evolution of the statistical parameters of the backscattering coefficients is not carried out on a pixel-by-pixel basis, but on homogeneous regions. To properly identify the homogeneous regions, the used segmentation must have the following properties:

- the segmented image is required to keep as much details as possible;
- shape of segments and edges should be obtained on the basis of all the images in the dataset, collected before and after the change occurrences.

To increase the change detection performance, we consider the use of a joint segmentation technique, to exploit both multi-temporal SAR and multi-spectral optical images at the same time. In particular, two alternative segmentation techniques are considered and compared in this paper:

- The first segmentation technique (SEGANN) is based on the maximization of the generalized likelihood of the whole set of SAR and optical images – which are assumed to be statistically independent –, by means of simulated annealing.
- The second segmentation (SEGIRR) is based on the idea of first performing line segmentations, and then reconstructing the segmented image by exploiting the irrotational property of a true gradient field. The temporal correlation among the images is taken into account.

A. Independent Segmentation Annealing (SEGANN)

The first segmentation technique is based on the statistical model in eq. (1). Based on this model, the generalized likelihood of the N_j, pixels of the *j-th* segment of the M SAR images, can be written as:

$$L_x^{(j)} = \prod_{n=1}^{N_j} \prod_{i=1}^{M} \frac{1}{\Gamma(\nu)} \left(\frac{\nu}{\eta_{j,i}} \right)^{\nu} x_{n,i}^{\nu-1} \exp\left(-\frac{\nu}{\eta_{j,i}} x_{n,i} \right) \tag{4}$$

Eq. (4) can be rewritten as

$$L_x^{(j)} = \left[e\, \Gamma(\nu) \right]^{-M N_j} \cdot \prod_{i=1}^{M} \left(\frac{\nu}{\eta_{j,i}} \right)^{\nu N_j} \cdot \prod_{i=1}^{M} \prod_{n=1}^{N_j} x_{n,i}^{(\nu-1)} \tag{5}$$

and in logarithmic form, as

$$\begin{aligned} \Lambda_x^{(j)} = & - M N_j - M N_j \ln\left[\Gamma(\nu) \right] + \\ & - \nu N_j \sum_{i=1}^{M} \ln\left(\frac{\nu}{\eta_{j,i}} \right) + (\nu - 1) \sum_{i=1}^{M} \sum_{n=1}^{N_j} \ln x_{n,i} \end{aligned} \tag{6}$$

Finally, the generalized likelihood over the whole image can be written as

$$\begin{aligned} \Lambda_x = & - M N - M N \ln\left[\Gamma(\nu) \right] + \\ & - \nu MN \ln \nu - \nu \sum_{i=1}^{M} \sum_{j=1}^{P} N_j \ln \eta_{j,i} + (\nu - 1) \sum_{j=1}^{P} \sum_{i=1}^{M} \sum_{n=1}^{N_j} \ln x_{n,i} \end{aligned} \tag{7}$$

being N the total number of pixels in each image. As apparent, eq. (7) depends not only on P and N_j, j=1, …, P, but also on the specific shape of the segments. These parameters can be obtained by maximizing the global generalized likelihood in eq. (7) by resorting to simulated annealing. This is effectively implemented by INFOSAR L.t.d., [5], in the INFOPACK SAR software tool.

The above described technique is described with reference to the M SAR images; however, it is easily extended to the whole set of SAR plus optical, when the number of looks of the SAR images is large enough. In fact, in this case the level of fluctuation of the SAR images around their mean value is not much larger than the fluctuation of the optical images around their mean value and both types of images can be approximately considered to share the same pdf in eq. (1). When this is the case, as for our dataset, eq. (7) is extended in a straightforward manner to the joint segmentation of SAR and optical images, by replacing the M SAR images with the M+3 images (M SAR images plus the three bands of the single optical image used in data set S2). In both cases, a shape parameter is used to apply a penalty for regions that have a small radius of curvature, so as to help the technique to converge to segments with smooth shapes. Moreover, over-segmented images are applied a merge stage to remove statistically inconsistent edges, [4].

1-4244-0712-5/07/$20.00 ©2007 IEEE.

B. Correlated Irrotational Segmentation (SEGIRR)

The second segmentation is based on the idea, introduced in [6], of splitting the original image segmentation problem in two sub-problems with lower computational complexity. First, a preliminary estimate of the segmented image gradient is found. A great simplification can be achieved by not requiring at this step that the obtained vector field is irrotational. This condition, which is necessary for a vector field to be a gradient, and then to reconstruct the segmented image as its line integral, is enforced successively as an independent problem. The computational advantage coming from the proposed decomposition can allow the implementation of sophisticated strategies that would be practically impossible to implement in a unique step. In particular, the 1D segmentations performed in the first step are based on a ML "region split" method, introduced in [6] for the segmentation of a single image, and extended here in order to obtain a joint segmentation of multiple SAR and/or optical data.

When the number of the looks L is high enough, the K-distribution characterizing the SAR statistic can be approximated by the lognormal distribution [4]. In particular, assuming absence of texture, the joint distribution of the logarithms z_n ($n=1,....,N_j$), of the pixel intensities for the *j-th* homogeneous region of N_j pixels can be written as the product of N_j identical Gaussian pdfs:

$$p_z(z_1,...,z_{N_j}) = (2\pi\sigma^2)^{-\frac{N_j}{2}} \exp\left(-\frac{1}{2\sigma^2}\sum_{n=1}^{N_j}(z_n-\mu)^2\right) \qquad (8)$$

where σ and μ encode the statistical information of the SAR reflectivity for the considered region.

Unlike SAR images, optical data have negligible noise levels and their pdf are essentially characterized by the radiance fluctuation in classes considered homogeneous. Moreover, the data collected at the different frequencies are likely to be highly correlated. From these considerations, the multivariate lognormal distribution in (8) can be considered an appropriate model to describe the joint pdf of the N pixels in a homogeneous region of the multi-channel optical image.

Combining the multivariate lognormal pdf functions characterizing SAR and/or optical data, the joint distribution of the multi-temporal SAR images and/or multi-band optical data, for a homogeneous region of Nj pixels, can be written as the multivariate Normal model of the logarithms:

$$p_{z^{(j)}}\left(\{\boldsymbol{\xi}_{n,j}\}\right) = \frac{1}{(2\pi)^{\frac{M'N_j}{2}}\left|\mathbf{R}\right|^{\frac{N_j}{2}}} e^{-\frac{1}{2}Tr\left\{\mathbf{R}^{-1}\sum_{n=1}^{N_j}(\mathbf{z}_n-\boldsymbol{\mu}_j)(\mathbf{z}_n-\boldsymbol{\mu}_j)^T\right\}} \qquad (9)$$

where $\boldsymbol{z}_n$ is the *M'*-dimensional vector formed by the M' logarithms of the SAR and/or optical pixel intensities in the homogeneous region. M' is the total number of images, with M'=M when considering the M SAR images only, and M'=M+3 when considering the M SAR images plus the three bands of an optical image. Moreover, the quantities $\boldsymbol{\mu}_j$ and $\boldsymbol{R}_j$ are respectively the M' dimensional mean values vector and the *M'xM'* dimensional covariance matrix.

A ML "region split" test based on (9) is used to split a region in two segments that have different statistics (hypothesis H_0) or to consider it a single homogeneous region (hypothesis H_1). As proposed in [6], the split test is applied to one-dimensional regions (rows or columns), from which the segmented image is reconstructed by enforcing irrotationality. The use of the multidimensional pdf (9) instead than a one-dimensional pdf (with the covariance matrices $\boldsymbol{R}$ instead than variances) extends the original technique proposed in [6], where a single image was segmented. This allows to exploit the information of the multitemporal SAR and/or multispectral optical data and their correlation.

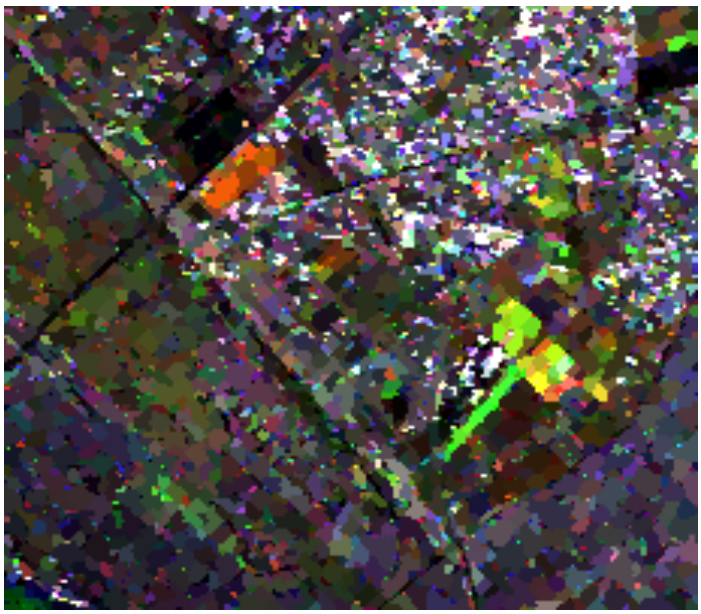

a)

b)

Figure 3: Segmentations (SM): a) SEGANN b) SEGIRR

In more details, consider a 1D region, that is a line of N_j pixels (on a row or on a column), partitioned in two contiguous and supposed uniform segments with respectively $N_{j,1}$ and $N_{j,2}$ pixels. In order to evaluate, by means of (9), the likelihood functions for both the hypotheses H_0 and H_1, the ML covariance matrixes $\boldsymbol{R}_{1,ML}$,$\boldsymbol{R}_{2,ML}$, for each region of respectively $N_{j,1}$ and $N_{j,2}$ samples, as well as the ML covariance matrix $\boldsymbol{R}_{0,ML}$, for the union of the two regions (with N_j samples), are calculated The comparison of the two evaluated likelihood functions, allows to decide between the hypothesis H_0 and H_1.

The region split procedure is applied iteratively. Initially, a line region (on a row or a column) of the image is analysed in order to look for an admissible partition by applying the "split region" test. If no admissible partitions are found, such region is considered a uniform segment. Otherwise, the region is split and the algorithm is applied again to the two just estimated segments. The algorithm works iteratively until when no edges are detected in all current segments.

The estimate of the 2D segmented image gradient obtained from the described 1D segmentation is not, in general, a true gradient. In fact, it is not an irrotational vector field that has a primitive function. Therefore, the gradient estimate is made irrotational by founding the minimum (according to a given metric) needed corrections. If the L_1 norm is used a robust solution can be found by solving a minimum cost flow problem on a network [7]. Finally, the segmented image can be evaluated by integrating the obtained irrotational gradient.

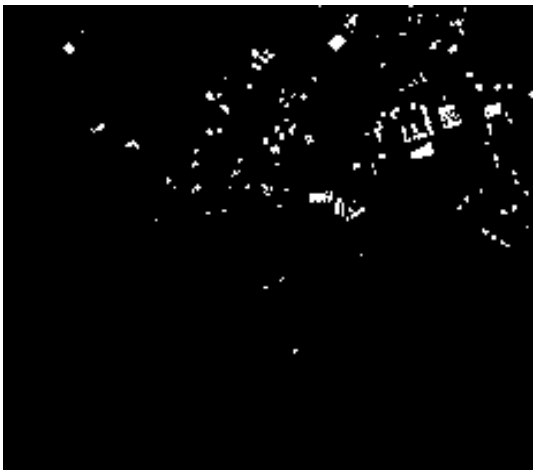

Figure 4: Truth Changes MAP (TM)

IV. Application to Real Data and Validation

The segmentation procedures have been applied to two sets of data (see Figure 3 for an example):

- Data Set 1 (S1): temporal series of 16 SAR images (ASAR/ENVISAT), acquired 10/11/2002 15/12/2002 30/03/2003 04/05/2003 17/08/2003 30/11/2003 18/04/2004 27/06/2004 01/08/2004 05/09/2004 10/10/2004 14/11/2004 19/12/2004 23/01/2005 05/04/2005 21/08/2005 and showing an area south of Rome.
- Data Set 2 (S2) temporal series of 16 SAR images in S1 and 1 multi-spectral (3 bands) optical data (Quick Bird) of the same scene acquired in August 2005.

In both cases, the segmentation results have been analyzed by comparing separately each SAR image to the global segmentation, to evaluate the obtained performance. In particular the ratio between the SAR images and the obtained segmentation is statistically analyzed in order to evaluate the quality of the despeckling and feature extraction processes. The approach to the evaluation is based on the fact that the speckle is a multiplicative noise with unity mean. Ideally, the ratio image should contain only speckle, but, in fact, it contains less speckle than expected, because residual speckle remains in the segmented image, and some features (i.e. edges, segments), which have been not captured by the segmentation. Based on above criteria, the ratio image for each SAR data ideally should have:

- *mean = 1*
- *variance = 0.577*, that is depending on the equivalent multi-look *L* (*variance=1/√L*, where in our case *L=3*).

When the variance is less than 0.577, a quantity of speckle is present in the segmented images; on the contrary, when values greater than 0.577 are found, some segments are expected to be missing in the segmented image.

TABLE I. Segmentation Results

Segmentation Type		**Statistics**
Data Set S1	Segmentation Level	***Variances***
SEGANN	Shape parameter s=0.00001	0.55
	Shape parameter s=0.01	0.46
	Shape parameter s=0.05	0.42
	Shape parameter s=0.1	0.40
SEGIRR	wide segments	0.55
	small segments	0.48
Data Set S2	Segmentation Level	***Variances***
S2	Shape parameter s=0.00001	0.54
	Shape parameter s=0.01	0.45
	Shape parameter s=0.05	0.41
	Shape parameter s=0.1	0.38
SEGIRR	wide segments	0.50
	small segments	0.42

In Table I the variances of the ratio image obtained for the S1 and S2 data set with different levels of segmentations, corresponding to different parameters in the SEGAN and SEGIRR procedures, are reported. The variances, reported in this table are averages of the variances obtained by considering all the 16 SAR images. As apparent, from a segmentation point of view, small shape parameters provide better performance for the SEGANN technique, the ratio images being most consistent

with the expected speckle statistic. In particular, very small shape parameters (about $s=10^{-5}$) allow to obtain variances of the ration images very close to the ideal value expected from speckle statistic. Analogously, better performance are obtained by the SEGIRR procedure when wider segments are searched.

In order to evaluate the performance of the change detection procedure, the S1 and S2 data sets and different segmentation maps (SM) are used, as reported in TABLE I.

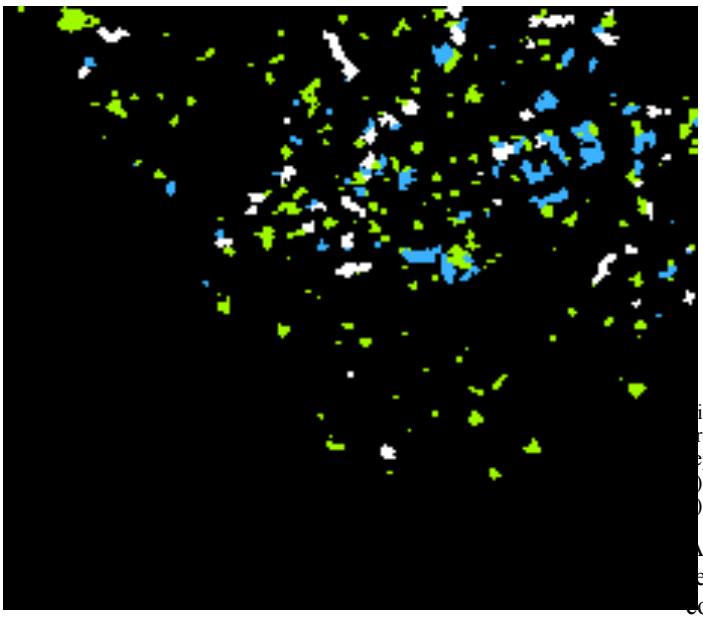

a)

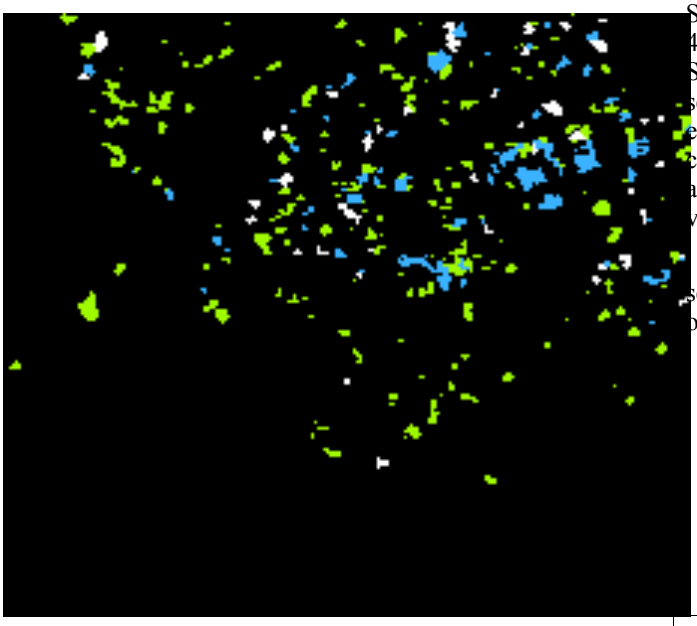

b)

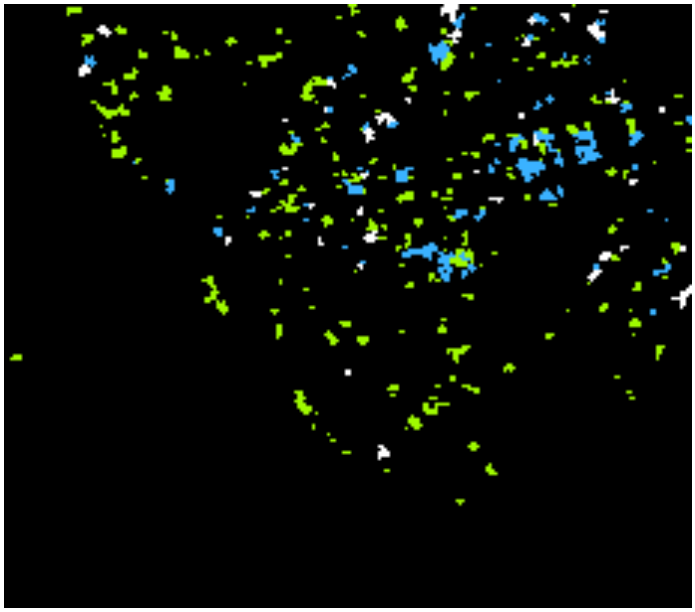

c)

igure 5: Validation results: green segments are false positive, blue segments re true positive, the white ones are the missed changes and the black areas epresent the true negatives. Validation results from S2 data set are shown in) for the shape parameter s=0.01 in b) for the shape parameter s=0.05 and in) for the shape parameter s=0.1

A map of the ground truth, reporting the real changes (TM) required by the validation, is obtained through visual comparison of two Quick Bird high-resolution optical images acquired at two different times, at the start and at the end of SAR multi-temporal series. This map is reported in Figure 4.The result of the change detection, applied to the selected SM, is a map of the changes (CM). In this map, for each segment of SM where a change has been detected, the estimated change time is reported. In CM, all segments corresponding to agricultural fields and highly vegetated areas are masked out in order to discard changes due to seasonal vegetation variations or to rain.

The validation of the proposed method has been performed segment by segment. Each segment in SM is classified in one of the following classes:

- true positive (TP), when a real change is detected;
- false positive (FP), when a in a change is erroneously detected;
- false negative (FN), when a change is missed;
- true negative (TN) in all remaining cases.

TABLE II. VALIDATION RESULTS

Segmentation Type		**Change Detection Results**	
Data Set S2	Segmentation Level	P_d	P_{fa}
SEGANN	Shape parameter s=0.01	70 %	3.3 %
	Shape parameter s=0.05	74.6 %	2,7 %
	Shape parameter s=0.1	77 %	2.2 %

Segmentation Type		Change Detection Results	
Data Set S2	Segmentation Level	P_d	P_{fa}
SEGIRR	Wide segments	69,2 %	2.7 %
	Small segments	72%	2.5 %

TABLE III. VALIDATION RESULTS

Segmentation Type		Change Detection Results	
Data Set S1	Segmentation Level	P_d	P_{fa}
SEGANN	Shape parameter s=0.01	65 %	4 %
	Shape parameter s=0.05	69.7 %	4 %
	Shape parameter s=0.1	73.5 %	2.9 %
SEGIRR	Wide segments	63 %	3 %
	Small segments	66.4 %	2.4 %

The CM determines if a segment of SM is positive, that is a change is detected, or negative. The validation of the positive or negative results on each segment in SM is obtained through a comparison with the TM. Since the segments in TM are not matching with the segments in SM, criteria of comparison are introduced, based on the estimation of the overlapping percentage between segments in TM and SM. In particular, if a SM segment is positive (that is, in CM a change has been detected), it will be classified as TP if its intersection with the corresponding TM is greater than 30% of its own area; Otherwise, the segment will be labeled as false positive. An analogous criterion is used to validate the negative segments in SM, where no changes have been detected. In Figure 5, Figure 6, Figure 7 and Figure 8 the CMs relative to S2 data set segmented with SEGANN, S2 data set segmented with SEGIRR, S1 data set segmented with SEGANN, S1 data set segmented with SEGIRR are reported, respectively.

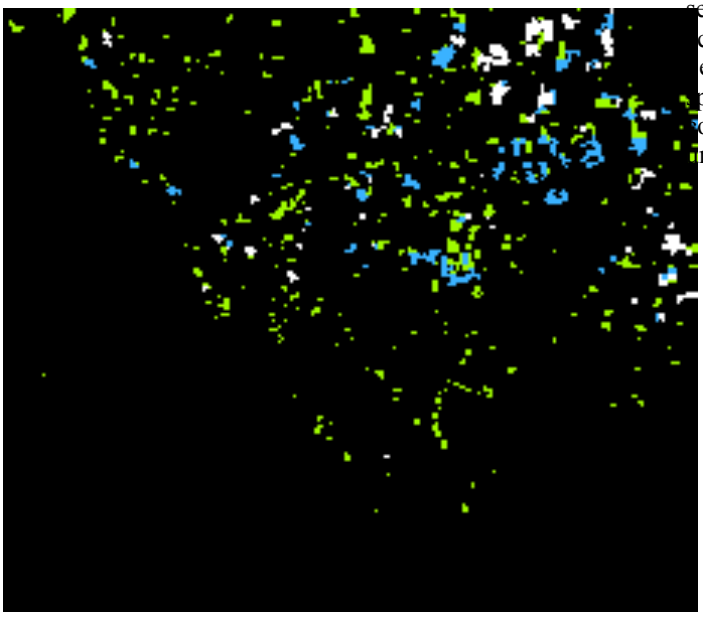

a)

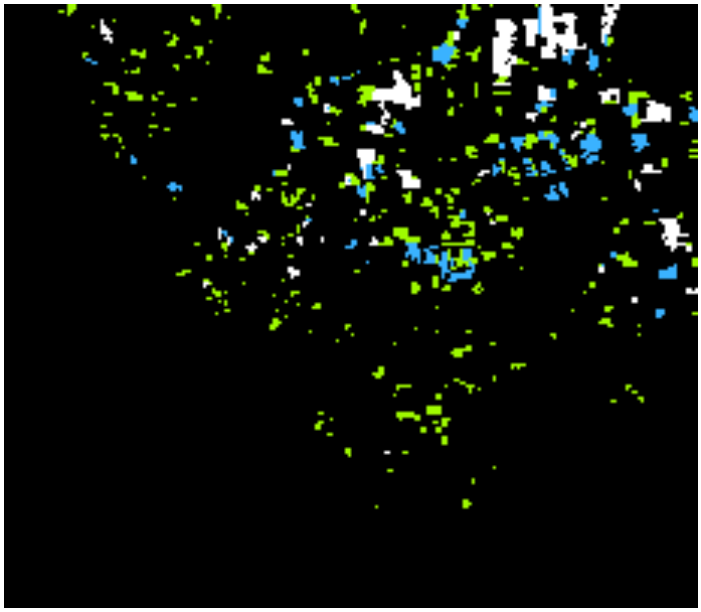

b)

Figure 6: Validation results: green segments are false positive, blue segments are true positive, the white ones are the missed changes and the black areas represent the true negatives. Validation results from S2 dataset SEGIRR are shown in a) for the small region segmentation and in b) for the wide region segmentation.

The effectiveness of the proposed technique is measured by evaluating the probabilities of detection and false alarm. The former is estimated as the detection rate: $P_d=N_{TP}/(N_{TP}+N_{FN})$, where N_{TP} is the number of true positive SM segments and N_{FN} is the number of the false positive ones. The latter is estimated by means of the false alarm rate: $P_{fa}=N_{FP}/(N_{FP}+N_{TN})$, where N_{FP} is the number of false positive SM segments and N_{TN} is the number of the true negative ones. The validation results are reported in TABLE II and in TABLE III for the data set S2 and S1, respectively. It can be noted that in both cases segmentations with smaller segments, even if not optimal according to the previously reported speckle criterion, lead to a better change detection performance. This might be due to the specific nature of the changes, which are related to the construction of infrastructures and buildings in a new area under development.

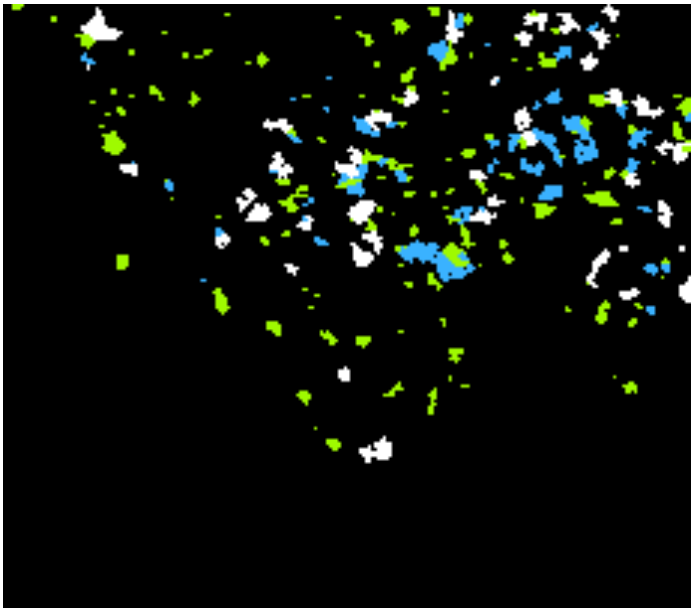

a)

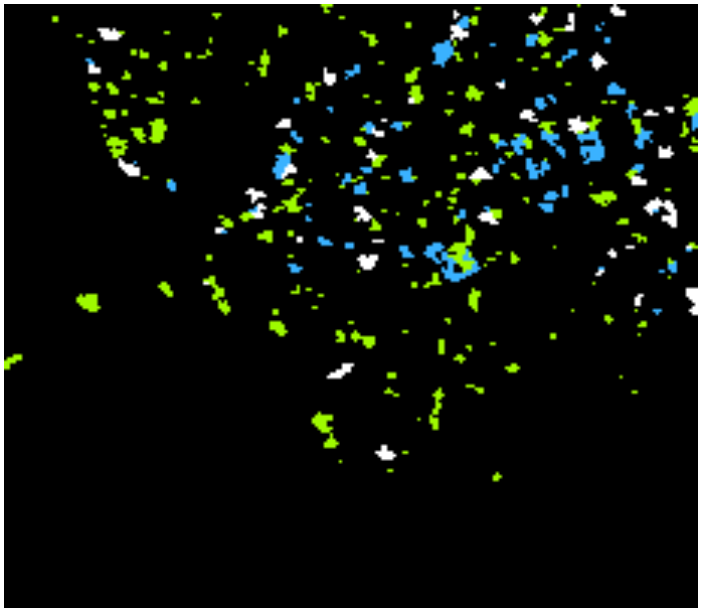

c)

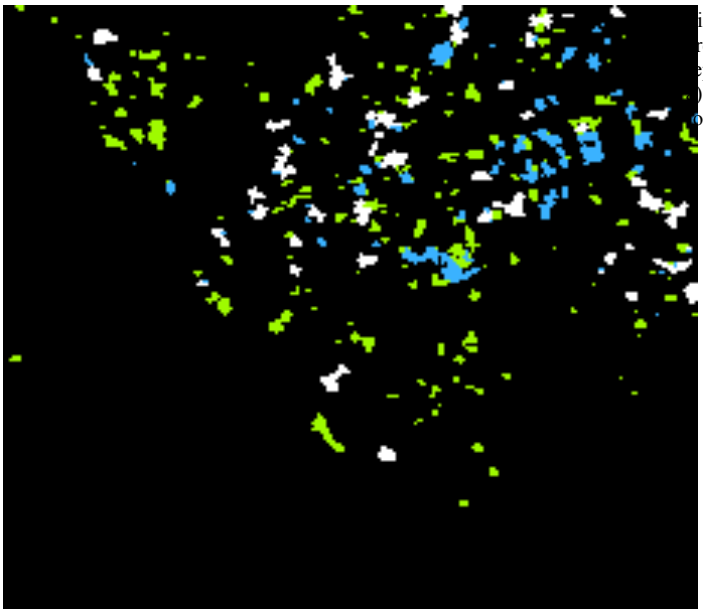

b)

igure 7: Validation results: green segments are false positive, blue segments re true positive, the white ones are the missed changes and the black areas epresent the true negatives. Validation results from S1 data set are shown in) for the shape parameter s=0.01 in b) for shape parameter s=0.05 and in c) or shape parameter s=0.1

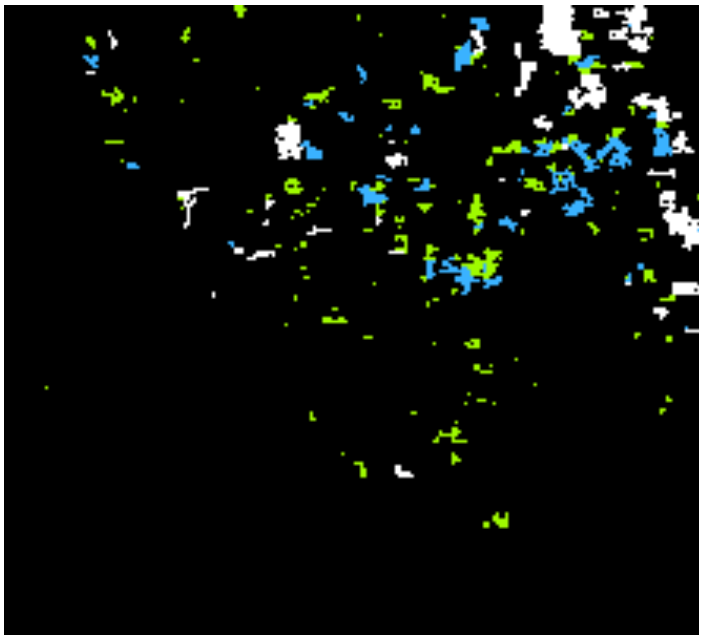

Figure 8: Validation results: green segments are false positive, blue segments are true positive, the white ones are the missed changes and the black areas represent the true negatives. Validation results from S1 dataset SEGIRR are shown for the small region segmentation.

Already in the general case, it is likely that a slight over-segmentation always provides better results than under-segmentation, since the larger number of small segments allows in general a better identification of details and borders. More specifically, when dealing with man-made objects, the non natural shape of the segments and the non-fully developed

1-4244-0712-5/07/$20.00 ©2007 IEEE.

speckle scenario can lead without surprise to better results with an over-segmented image.

Despite the presented results are preliminary, it appears that considering the correlation between the different images, as done by the SEGIRR algorithm, does not lead to better results than using the simple statistical model of SEGANN. This could be due to the fact that SEGANN uses a global approach instead than a two-steps approach like SEGIRR. However, better change detection results than those reported in TABLE II were obtained in tests where the SEGIRR algorithm was used considering the different images as independent (diagonal covariance matrices $\boldsymbol{R}$ in (9)). A possible explanation of this fact is that the exploitation of the correlation among the employed data is an hard task, due to the smearing of the information which make difficult an ML estimation of the covariance matrices for small segments (particularly when many images are used). This could lead SEGIRR to be less performing in exploiting the information in small segments as those characterizing buildings, which are likely candidate to be subject to changes. For this reason, more sophisticate shrinkage methods should be taken into account by introducing opportune models in order to estimate the covariance matrices.

While the achieved results need to be improved in terms of probability of correct classification, both by refining the knowledge of the ground truth and by improving the segmentation results, the exploitation of optical images in the change detection process allows a significant improvement in the segmentation and therefore in the change detection quality.

V. Conclusions and Future Work

Two approaches to the joint segmentation of SAR and optical images have been studied and compared, used as the preliminary basic step required of a procedure aimed at detecting changes and estimating their time of occurrence inside a temporal series of SAR images. The change detection technique does not require "a priori" knowledge on the change time and on the RCS levels before and after the change in the SAR images. While one segmentation approach uses a highly reliable segmentation annealing approach, the other uses a more complex statistical model in order to take into account the correlations between the different images. In both cases, segmentations with smaller segments, even if not optimal from the point of view of the segmentation quality, lead to a better change detection performance. However, the present study is preliminary and leaves room for a significant improvement of the change detection performance, when a large sequence of SAR images is available.

The exploitation of optical images together with SAR data allows to obtain a rich and sharp segmentation, which is the basis of the statistical approach to estimate the changes. Indeed, an accurate knowledge of the homogeneous regions given by the joint segmentation allows a better exploitation of the whole available information for detecting step pattern changes in the segments. Robustness in the exploitation is still an issue which requires future work.

The preliminary results shown in this paper, obtained processing ENVISAT SAR and Quick Bird optical data, demonstrate the validity of the proposed technique, thought further improvements can be introduced. In particular, different change patterns (other than the step change) can be introduced in the change detection technique. Moreover, multiple optical images acquired at different times, if available, can be employed to perform a more effective change detection. These points will be topics for future works of the authors.

References

[1] P. Lombardo, C.J.Oliver, T.Macrì Pellizzeri, M.Meloni, "A new maximun-likelihood joint segmentation technique for multitemporal SAR and multiband optical images," IEEE *Transaction on Geoscience and Remote sening*, vol. 41, no. 11,pp. 2500-2518, November 2003.

[2] P.Lombardo, T. Macrì Pellizzeri, "Maximum likelihood signal processing techiniques to detect a step pattern of change in multitemporal SAR images," *IEEE Transaction on Geoscience and Remote sening*, vol. 40, NO. 4, pp. 853–870, April 2002.

[3] P.Lombardo, T. Macrì Pellizzeri, "Localization of step changes in multitemporal SAR images," *IEEE Transaction on Aerospace and Eletronic Systems*, vol. 38, NO. 4, pp. 1256–1275, October 2003.

[4] C.J.Oliver and S.Quegan, *Understanding SAR images*. Boston, MA: Artech House, 1998.

[5] http://www.infosar.co.uk/

[6] M. Costantini, M.Zavagli, M. Milillo, "*A novel approach for image segmentation*", IGARSS '02. Proceedings. 2002 IEEE International.

[7] M. Costantini, "A Novel phase unwrapping method base on network programming," ," IEEE *Transaction on Geoscience and Remote sening,* vol 36, No 3, pp 813-821 May 1998.